frontiers | Frontiers in Membrane Science and Technology

TYPE Original Research
PUBLISHED 10 October 2023
DOI 10.3389/frmst.2023.1247276

OPEN ACCESS

EDITED BY
Maria Giovanna Buonomenna,
Ordine dei Chimici e Fisici della Campania and MIUR, Italy

REVIEWED BY
Mohamed Khayet,
Complutense University of Madrid, Spain
Nurasyikin Misdan,
Universiti Tun Hussein Onn Malaysia, Malaysia

*CORRESPONDENCE
Lebea N. Nthunya,
nthunyalebea@gmail.com
Heidi Richards,
Heidi.richards@wits.ac.za

RECEIVED 25 June 2023
ACCEPTED 29 September 2023
PUBLISHED 10 October 2023

CITATION
Chimanlal I, Nthunya LN, Quist-Jensen C and Richards H (2023), Resource recovery from acid mine drainage in membrane distillation crystallization. *Front. Membr. Sci. Technol.* 2:1247276. doi: 10.3389/frmst.2023.1247276

Resource recovery from acid mine drainage in membrane distillation crystallization

Indira Chimanlal[1,2], Lebea N. Nthunya[1,2]*, Cejna Quist-Jensen[2] and Heidi Richards[1]*

[1]Molecular Sciences Institute, School of Chemistry, University of Witwatersrand, Johannesburg, South Africa, [2]Department of Chemistry and Bioscience, Center for Membrane Technology, Aalborg University, Aalborg, Denmark

Acid mine drainage (AMD) remains a global threat with no exception to South African water bodies and the environment. It promotes environmental challenges with emerging concerns on water security and drinking water pollution. This study evaluated membrane distillation crystallization (MDC) towards resource recovery from AMD. To ensure high process performance, polyvinylidene fluoride (PVDF) membranes evaluated in the current study were modified using hydrophobic nanoparticle additives and compared with PTFE-20 reference membrane. The produced permeate flux of PTFE-20 reference membranes and M4 ($fSiO_2$NPs-modified membrane) were 2.426 kg m^{-2}·h^{-1} and 1.459 kg m^{-2}·h^{-1}, respectively. Similarly, salt rejections were 99.96% and 97.52%, respectively. Based on single crystal x-ray diffraction and scanning electron microscopy analysis, MDC predominantly produced monoclinic gypsum ($CaSO_4.2H_2O$) with the C2/c space group. Also, crystal properties obtained in $fSiO_2$NPs-modified and PTFE-20 reference membranes were comparable. Though a considerable amount of gypsum was obtained, membrane surfaces were characterized by traces of salt deposit, with possible membrane scaling leading to performance deterioration. The permeate conductivity increased rapidly at the highest water recovery factor, indicating membrane wetting caused by scaling.

KEYWORDS

membrane distillation crystallization, resource recovery, fouling, silica nanoparticles modification, process performance

Highlights

- Nanoparticle-modified PVDF membranes were prepared via phase separation process.
- To improve process performance, the membranes were modified with fCNTs and fSiO2NPs.
- The hydrophobic PVDF membranes were evaluated towards resource recovery in membrane distillation crystallization.
- Performance of prepared membranes was compared to PTFE-20 reference membrane.
- High salt rejection and water flux were recorded for fSiO2NPs-modified membranes and PTFE-20 reference membrane.
- Various crystal minerals including gypsum were recovered in membrane distillation crystallization.

1 Introduction

An increased global population has caused rising demand for natural resources. This is propelled by the need for minerals in the wake of evolving industries and economic sectors. Consequently, a larger amount of waste is generated in tandem with greater industrial output. Upon disposal without adequate treatment, wastewater discharged from industries cause disastrous implications on the environment and human health (Yadav et al., 2022). Produced water from oil and gas extraction (Ali et al., 2015), acid mine drainage (AMD), and brines introduce large volumes of salt into the environment. These polluted wastewaters are characterized by toxic chemicals, negatively impacting the environment, humans, animals, and microorganisms (Anekwe and Isa, 2023). The consequences thereof include plant dehydration, nutrient and hormonal imbalances, and environmental toxicity, among others (Ondrasek and Rengel, 2021; Stein et al., 2021). When left untreated, wastewater causes biomagnification in aquatic and terrestrial environments (Dhamsaniya et al., 2022). Accordingly, freshwater sources are declining due to progressive environmental contamination and exploitation (Greve et al., 2018). Among others, landfill leachates and AMD are the major drivers posing a threat to drinking water security and pollution. This is no exception in South Africa since the inception of mining activities and domestic landfill. Leachate wastewater is defined as water percolating through waste and contains a high level of unwanted chemicals (Dhamsaniya et al., 2022). The AMD is typically generated when sulphide materials react with oxygenated water and air. Moreover, this type of wastewater is detrimental to surrounding ecosystems due to high levels of iron and sulphate in conjunction to its low pH (Alegbe et al., 2019).

Therefore, remedial technologies are required to alleviate the AMD wastewater. The abundance of minerals found in these waste streams provides an opportunity for their recycling and reuse. This is vital as it encourages circular economies, reduces the quantity of waste introduced to the environment, and improves the quality of discharged water to save the environment. Reverse osmosis is a mature technology commonly used to treat high saline waters. To minimize fouling, RO feed water is treated using low pressure ultrafiltration (UF) and microfiltration (MF). During water softening, nanofiltration (NF) is commonly used. However, these technologies have limitations such as high operating pressures leading to high treatment expenditures (Ali et al., 2015; Lu et al., 2017). For these reasons, they are rarely exploited in developing countries. Furthermore, RO produces concentrated brines with low recovery factors (40%–50%), creating disposal challenges. Other treatment strategies often employed to alleviate the environmental expense include electrodialysis (Akcil and Koldas, 2006), passive bio-reactors (Akcil and Koldas, 2006), adsorbents (Egashira et al., 2012; Chimanlal et al., 2022b), and biological treatments (Dhamsaniya et al., 2022). In addition to economic challenges, fouling and process inefficiency are key factors affecting their use in industrial wastewater treatment.

Membrane distillation (MD) was introduced as a promising technology to address challenges facing pressure-driven water treatment technologies. When integrated with conventional crystallization, MD can recover freshwater and minerals from wastewater. This emerging technology is known as membrane distillation crystallization (MDC). MDC is a thermal process facilitating separation through a hydrophobic membrane. Technically, the water passes through the membrane in vapor form, exclusively retaining solutes and minerals (Lu et al., 2017). The hot and cold interfaces from different sides of the membrane establish a vapor pressure gradient acting as the driving force. In MDC, the feed solution is concentrated to supersaturation thus facilitating mineral recovery through crystallization. During MDC applications, the hydrophobic membrane plays two roles, namely; 1) provision of a mass transfer interface to concentrate the feed solution through solvent evaporation, and 2) promotion of heterogeneous nucleation (Edwie and Chung, 2013; Jiang et al., 2016). This technology possesses various advantages including treatment of highly concentrated feed streams, utilization of renewable energy and is less energy intensive. Additionally, MDC affords well-controlled supersaturation rates, crystal nucleation, and growth (Sparenberg, Ruiz Salmón and Luis, 2020). Most interestingly, MDC can simultaneously recover minerals and freshwater in one process (Yadav et al., 2022). Unfortunately, MDC is affected by fouling/scaling due to contaminant deposition on the membrane surface or within its pores resulting in a deteriorated membrane performance (Gryta, 2008; Nthunya et al., 2019). Membrane wetting is another challenge commonly affecting the quality of recovered water (Chimanlal et al., 2022a). To ensure high process performance, various hydrophobic membranes originating from a variety of sources (commercial or synthetic) are often used in MDC systems. This work evaluated the recovery of freshwater and minerals in MDC using synthesized PVDF hydrophobic membranes and a commercial PTFE reference membrane. Our previously reported PVDF membranes (M3 and M4) modified with respective fCNTs and $fSiO_2$NPs were used in the current study (Chimanlal et al., 2023). Simulated AMD was used as a feed solution. The MDC evaluation towards treatment of these types of wastewaters will encourage research addressing issues of water scarcity, environmental pollution, and circular economy.

2 Methods and materials

2.1 Reagents

Certified aqueous reference cation multi-element standard and anion reference standard solutions (1,000 mg L^{-1}) were obtained

TABLE 1 Composition of the synthesized membranes evaluated in the current study.

Membrane	DMF	DMAc	PVDF (wt%)	PVP (wt%)	fCNTs (wt%)	$fSiO_2$NPS (wt%)
M3	50.8	33.9	15.0	0.1	0.2	0.0
M4	48.7	32.5	15.0	0.1	0.2	3.5

TABLE 2 Composition of the synthetic AMD solution used for MDC.

Salt	Concentration (mg L^{-1})
NaCl	89.68
$CaSO_4$	301.6
$CoSO_4$	10.52
$ZnSO_4$	64.03
$Fe_2(SO_4)_3$	981.0
$MgSO_4$	1617.3
K_2SO_4	325.4
$NiSO_4$	17.67
NaF	10.83
$Al_2(SO_4)_3$	253.6

from De Bruyn Ultraspec (Johannesburg, South Africa). Materials used for membrane fabrication included polyvinylidene fluoride (PVDF, MW = 534,000 mg mol^{-1}), dimethylformamide (DMF, 90.0%), dimethylacetamide (DMac, 99.0%), and polyvinylpyrrolidone as the pore former (PVP MW = 360,000 mg mol^{-1}). All reagents were purchased from Sigma-Aldrich (Johannesburg, South Africa). A commercially acquired PTFE membrane with a pore size (0.20 µm) supported on non-woven polyester was provided by Pall Corporation (New York, United States).

2.2 Membrane synthesis

Detailed preparation and modification of PVDF membranes was reported elsewhere (Chimanlal et al., 2023). The previous membranes were evaluated towards seawater desalination in membrane distillation. For the purpose of the current study, high performance fCNTs and $fSiO_2$NPs modified membranes, namely M3 and M4 were selected (Chimanlal et al., 2023). Briefly, an appropriate amount of PVDF was dispersed in a mixed solvent system of DMac/DMF (2:3) and stirred for 24 h. Following a degassing, the solution was cast on a glass plate and immersed into a water bath to promote phase separation. The fCNTs and $fSiO_2$NPs were dispersed into the cast solution prior to the degassing. To ensure particle dispersion, the cast solutions were sonicated using Eins Sci Profession ultrasonic cleaner under the normal setting (Johannesburg, South Africa). The fCNTs and $fSiO_2$NPs-modified membranes were termed M3 and M4 as per previous study. Table 1 provides the composition of the prepared membranes.

2.3 Evaluation of membrane distillation crystallization process performance

For all MDC experiments, a feed solution resembling characteristics of AMD was utilized. (Table 2). The synthetic solution was prepared from a mixture of different salts, namely; sodium chloride (NaCl), sodium fluoride (NaF), potassium sulfate (K_2SO_4), nickel sulfate ($NiSO_4 \cdot 6H_2O$), cobalt chloride ($CoCl_2 \cdot 6H_2O$), zinc sulfate ($ZnSO_4 \cdot H_2O$), calcium nitrate ($Ca(NO_3)_2 \cdot 4H_2O$), ferric sulphate ($Fe_2(SO4)_3 \cdot {}_xH_2O$), and anhydrous magnesium sulfate ($MgSO_4$). To adjust pH of the feed solution, 0.1 M nitric acid (HNO_3) and sodium hydroxide (NaOH) were used. The feed and permeate solutions were circulated in MD co-current configuration at 60 °C and 10.0 °C, respectively. A membrane area of 152 × 110 mm^2 was used, along with a crossflow velocity of 524 mL min^{-1}. The change in mass and conductivity of the permeate was measured continuously using Latitude Compact bench scale (Johannesburg, South Africa) and Hanna benchtop multiparameter meter (Washington, USA) respectively. Upon supersaturation, the feed solution was placed into an ice bath, followed by filtration, and drying. Distillate flux J) was calculated using Eq. 1, where Δm is the difference in the permeate mass (kg), Δt is the time difference (h) and A is the membrane area (m^2). After MDC process evaluation, used membranes were analyzed to understand their interaction with the feed solutions. Morphological properties of the salt crystals and

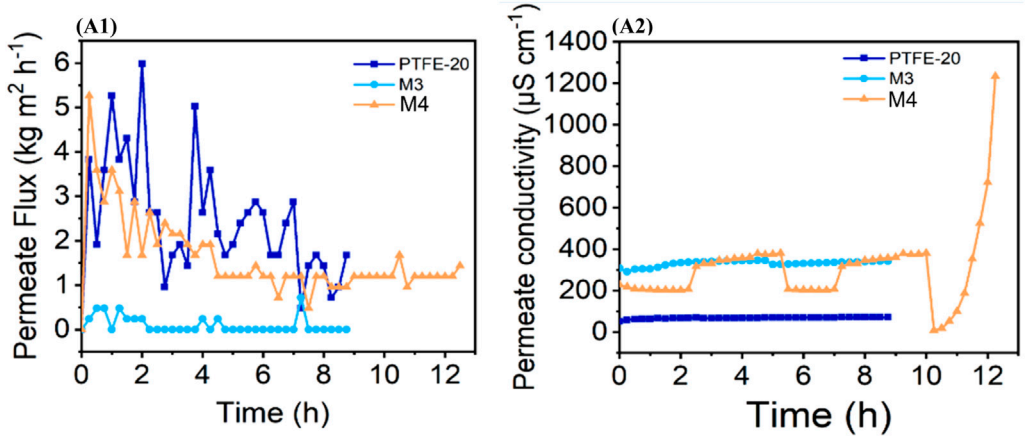

FIGURE 1
(A1) Permeate flux of the evaluated membranes and **(A2)** their corresponding conductivity profiles.

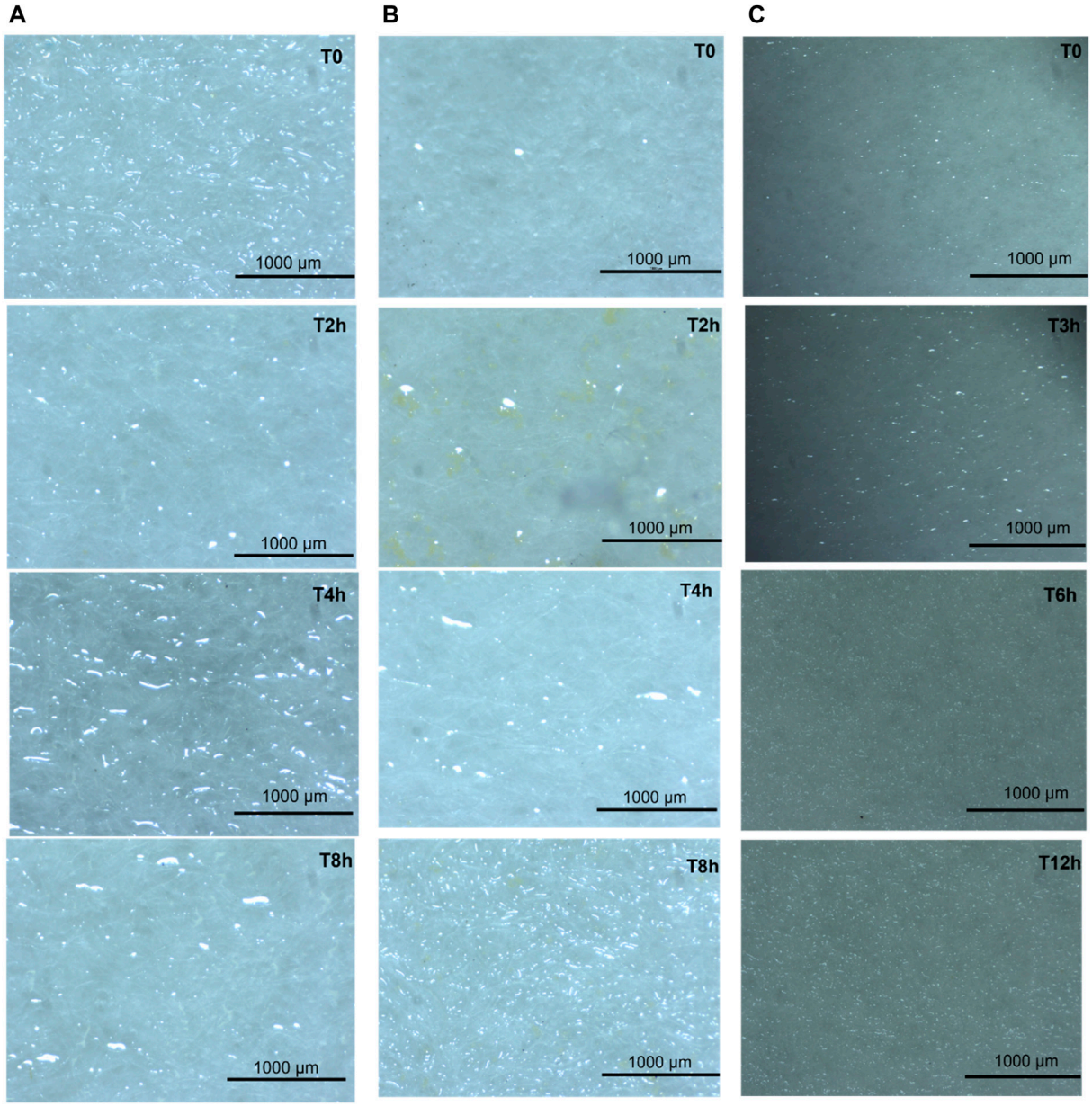

FIGURE 2
Micrographs depicting crystal development during MDC using membranes **(A)** PTFE-20, **(B)** M3, and **(C)** M4.

membranes were acquired from TESCAN Vega scanning electron microscopy (SEM, Libušina, Czech Republic) at 30.0 kV. All samples were coated with one layer of carbon and Au/Pd before analysis. Elemental mapping of the used membranes was obtained from Energy Dispersive Spectroscopy (EDS) coupled with SEM.

$$J = \frac{\Delta m}{\Delta t^{*} A} \tag{1}$$

2.4 Crystal characterisation

To evaluate the crystal formation, samples were collected at 30 min intervals and analyzed using the Nikon stereoscopic microscope SMZ745T equipped with NIS elements Imaging software (Tokyo, Japan). Produced crystals were analyzed using powder x-ray diffraction (PXRD, Bruker D2 Phaser Diffractometer equipped with a non-monochromated Co-Kα source, λ = 1.785 Å). Single crystals generated with PTFE-20 and M4 were analyzed using Bruker D8 Venture Bio PHOTON III 28-pixel array area detector (208 × 128 mm^2) diffractometer, coupled with a Mo Kα IμS DIAMOND source (50kV, 1.4 mA). The analysis was performed at 173 K. The unit cell and complete data set were obtained using *APEX4* (Bruker, 2021) and integrated using *SAINT*. The *SADABS* was used to evaluate empirical adsorption corrections and data scaling. Furthermore, using Olex2 (Dolomanov et al., 2009), the respective crystal structures were resolved with *ShelXT* (Sheldrick, 2015b) and refined using *ShelXL* (Sheldrick, 2015a). All database

TABLE 3 Crystallographic information for gypsum obtained with PTFE-20 and M4.

Crystal data	PTFE-20	M4
Empirical formula	CaH_4O_6S	CaH_4O_6S
Formula weight	172.17	172.17
Temperature (K)	173.00	173.00
Crystal system	monoclinic	monoclinic
Space group	C2/c	C2/c
a (Å)	6.2633 (3)	6.2626 (6)
b (Å)	15.1323 (8)	15.1313 (12)
c (Å)	5.6715 (3)	5.6692 (4)
α (°)	90	90
β (°)	490.25	114.201 (3)
γ (°)	90	90
Volume (Å^3)	490.25 (4)	490.01 (7)
Z	4	4
ρ_{calc} (g cm^{-3})	2.333	2.334
μ (mm^{-1})	1.648	1.649
F (000)	352.0	352.0
Crystal size (mm^3)	0.379 x 0.084 x 0.077	0.259 x 0.058 x 0.038
Radiation	MoKa (λ = 0.71073)	MoKa (λ = 0.71073)
2Θ range for data collection (°)	5.384 to 56.754	5.384 to 56.554
Index ranges	-8 ≤ h ≤ 8, -20 ≤ k ≤ 20, -7 ≤ 1 ≤ 7	-8 ≤ h ≤ 8, -20 ≤ k ≤ 20, -7 ≤ 1 ≤ 7
Reflections collected	4240	8403
Independent reflections	599 [R_{int} = 0.0381, R_{sigma} = 0.0254]	610 [R_{int} = 0.0897, R_{sigma} = 0.0399]
Data/restraints/parameters	599/1/46	610/1/44
Goodness-of-fit on F^2	1.220	1.186
Final R indexes [I>=2σ (I)]	R_1 = 0.0275, wR_2 = 0.0688	R_1 = 0.0330, wR_2 = 0.0854
Final R indexes [all data]	R_1 = 0.0281, wR_2 = 0.0692	R_1 = 0.0353, wR_2 = 0.0889
Largest diff. peak/hole/e Å^{-3}	0.41/-0.53	0.33/-0.69

files were retrieved from ICSD crystal. Furthermore, all PXRD refinements and database matching was performed using BRUKER DIFFRAC. TOPAS V7.20 software.

3 Results and discussions

3.1 Freshwater and mineral recovery in membrane distillation crystallization

Membrane distillation crystallization (MDC) was evaluated towards the recovery of freshwater and minerals from synthetic AMD wherein three membranes (M3, M4 and PTFE-20) were assessed at 60 °C feed temperature (Figure 1). The average permeate flux of PTFE-20 and M4 were 2.426 and 1.459 kg m^{-2}·h^{-1}, respectively. Additionally, the salt rejections were 99.96% and 97.52% for the respective membranes. The reference membrane (PTFE-20) produced the highest permeate flux, attributed to its integral structural with minimal defects (Chimanlal et al., 2023). However, M3 presented the lowest performance (Figure 1A1). Due to low water recovery rate, it was incapable of attaining supersaturation, and thus did not produce any crystal product. Moreover, membrane performance was affected by surface deposition as evidenced by SEM micrographs (Figure 3B). Notably, salt deposition on the membrane surface altered its structural integrity, thus leading to its poor performance (Choi et al., 2020). Nonetheless, M4 was susceptible to flux decline over time, attributed to feed temperature and cross flow velocity changes to their critical values (Zhao et al., 2011). Notably, M4 was characterized by a deposition layer (Figure 3 C). However, its impact on flux decline was minimal. The M4 was modified with fluorosilanized hydrophobic fSiO_2NPs, capable of reducing interfacial free energy of the membrane (Chimanlal et al., 2023). Reduced

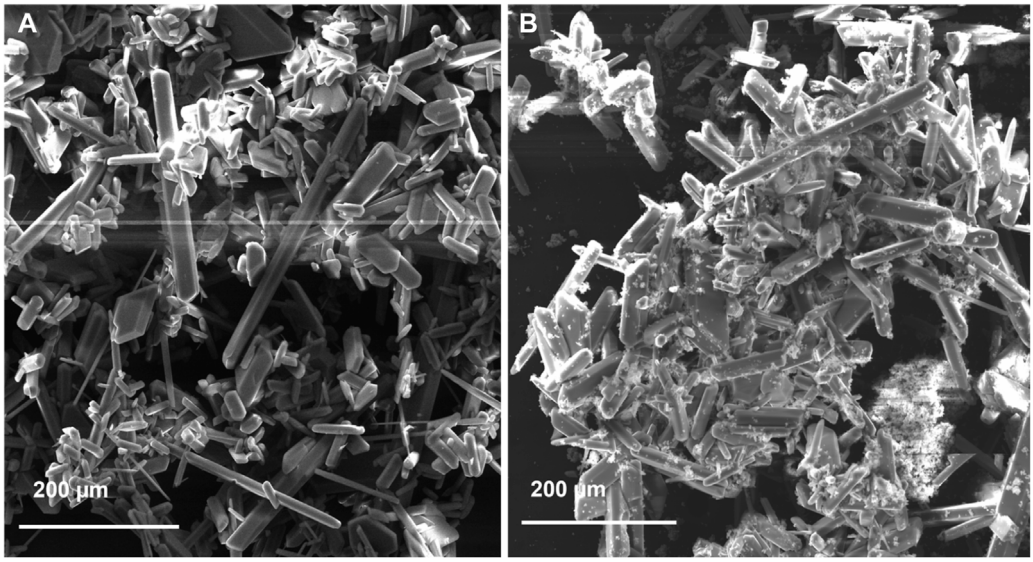

FIGURE 3
SEM micrographs showing crystal morphology following MDC tests using **(A)** PTFE-20 **(B)** M4.

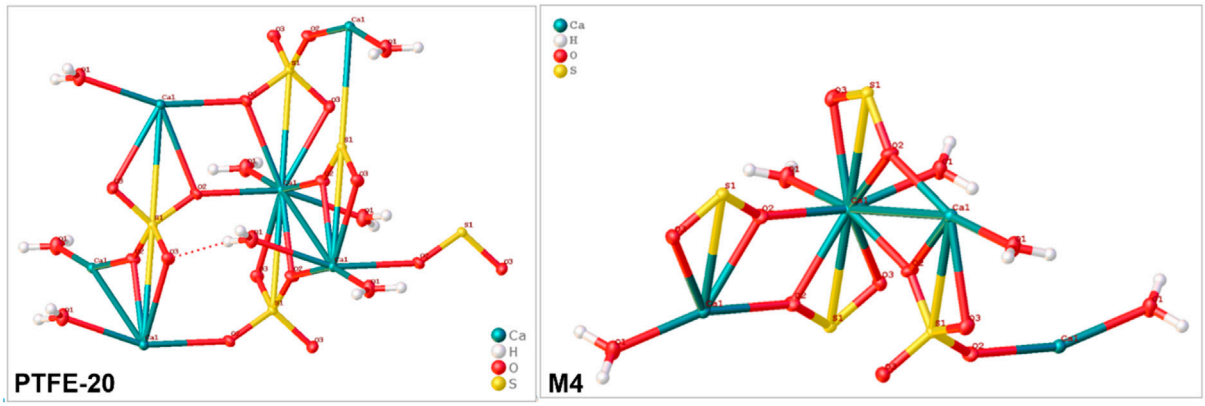

FIGURE 4
Crystal structures of gypsum produced with PTFE-20 and M4, respectively.

interfacial energy lowered bonding interaction between the NP and the inorganic salts in the feed solution (Gontarek-Castro et al., 2022). Resultantly, membrane resistance to fouling and wetting was reduced compared to M3.

Salt deposition near the membrane-feed interface diminished the liquid-vapor boundary leading to a swift flux and salt rejection decline (Edwie and Chung, 2013). Compounded to this, temperature polarization could be another contributing factor towards flux decay (Olatunji and Camacho, 2018). Moreover, a reduced temperature at the membrane interface lowered vapor pressure, thus causing a decay in distillate flux (Edwie and Chung, 2013). Interestingly, incorporation of $fSiO_2$NPs (i.e., M4) improved process performance considerably. The hydrophobicity of the $fSiO_2$NPs delayed the onset of membrane wetting. Precisely, M4 presented resistance to salt rejection decay and flux decline at low water recoveries prior to solution saturation. Evident from the previous reported findings, $fSiO_2$NPs improved membrane surface roughness and increased liquid entry pressure, rendering it more hydrophobic with improved resistance to wetting compared to M3 (Chimanlal et al., 2023). However, due to lower recovery rate compared to PTFE-20, M4 required a lengthy duration to reach supersaturation. Also, a gradual increase in the distillate conductivity recorded on M4 suggested the onset of membrane wetting (Figure 1 A2). Nonetheless, a satisfactory salt rejection was recorded (97.52%).

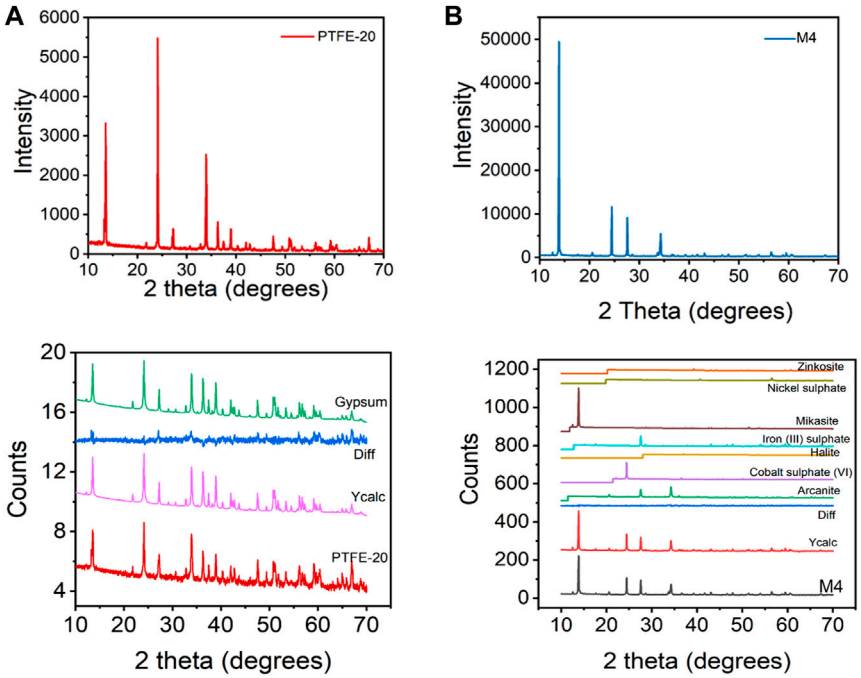

FIGURE 5
Experimental PXRD patterns for using **(A)** PTFE-20 and **(B)** M4 and their corresponding database plots.

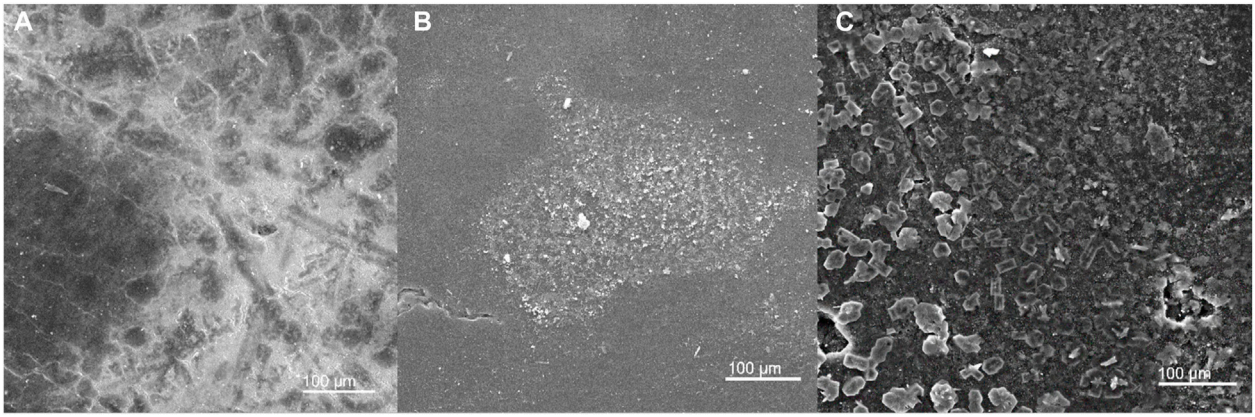

FIGURE 6
SEM micrographs depicting deposition on the membrane surface of **(A)** PTFE-20, **(B)** M3, and, **(C)** M4.

3.2 Crystal analysis

3.2.1 Microscopic imagery

Upon saturation of the feed solution, crystal formation was assessed microscopically (Figures 2A–C). The micrographs presented the formation of crystals as the solution gradually reached supersaturation. Micrographs obtained using PTFE-20 (Figure 2A) presented needle-like orthorhombic crystals with possible elongation at higher process duration (t = 4 h) (Alvarez et al., 2020). Based on the microscopic image, the number of crystals forming increased linearly with time (Figures 2B,2). The M4 produced elongated and needle-like crystals compared to those produced from PTFE-20. Although M3 exhibited poor MDC performance, it enabled minimal gel-like crystals (Figure 2B).

Apart from the oxidized form of iron, AMD consists of a wide range of mineral salts crystallizing in various forms (García-Lorenzo et al., 2016). Figure 3 presents SEM micrographs of the obtained crystals. The PTFE-20 and M4 produced crystals of varying sizes with a cubic-like crystal structure. Similar findings were reported by Choi et al. (2018). However, XRD presented minor differences in crystallinity of the obtained minerals for M4 and PTFE-20 (Table 3). Small changes in the morphology and crystal structure between the

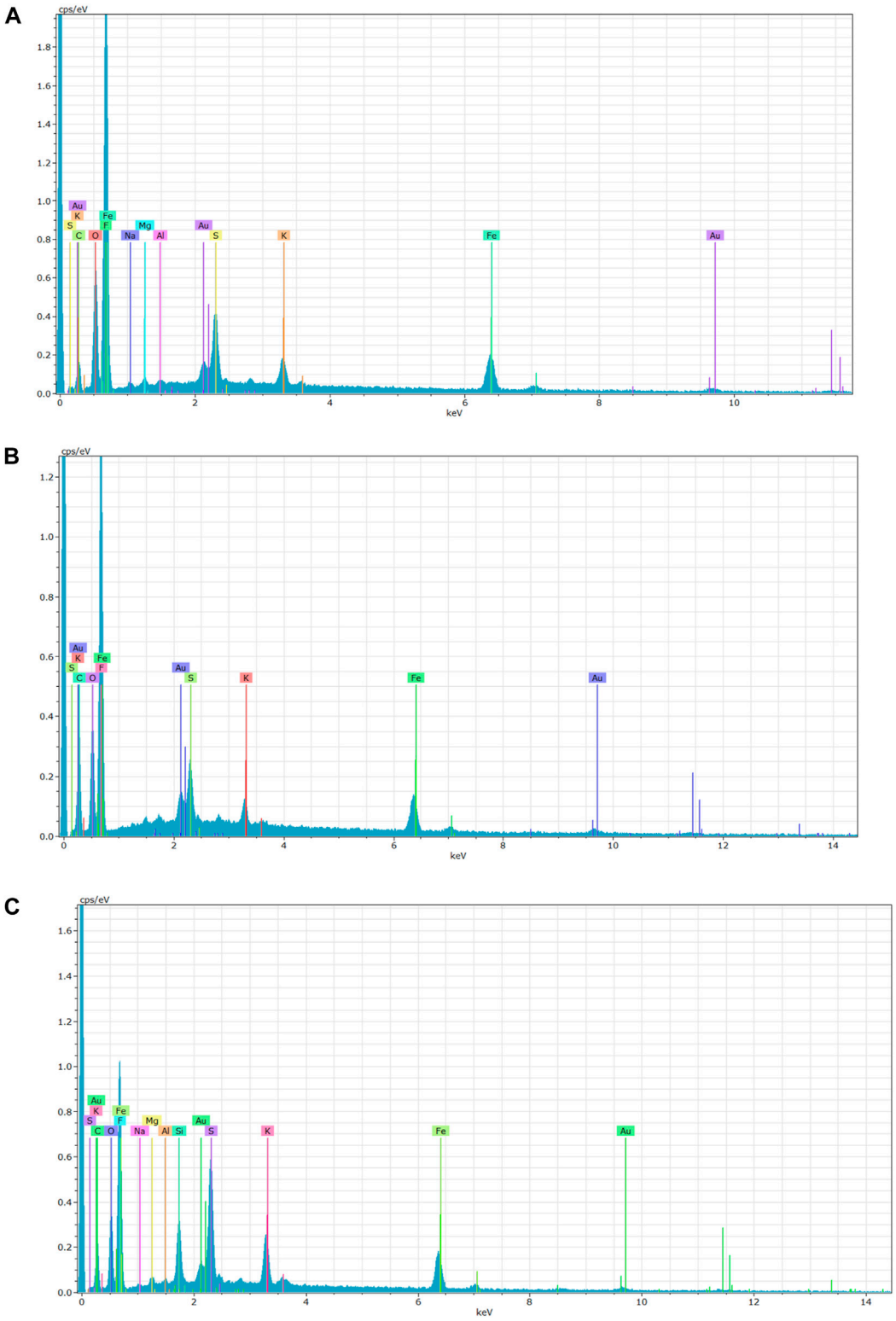

FIGURE 7
EDS spectra showing the elemental composition of membrane fouling deposition on **(A)** PTFE-20, **(B)** M3, and, **(C)** M4.

two products was attributed to chemical reaction or physical factors (such as agitation speed) (Choi et al., 2018). Notably, crystals were not formed upon use of M3. This was attributed to its low rate of water recoveries.

3.2.2 Crystal structure refinement and identification

Single crystal x-ray diffraction (XRD) was used to assess the type of minerals produced for each membrane (PTFE-20 and M4).

Reduced membrane wetting facilitated feed concentration, with subsequent crystal nucleation and growth. Although commercial membranes ensure high salt rejection, promoting crystal formation, improved membrane hydrophobicity is key in MDC. Technically, crystallized salts deposited on the membrane surface promote wetting of the adjacent pores. However, wetting phenomena is reducing by incorporating $fSiO_2$NPs (M4). In the current study, the dominant mineral produced was gypsum ($CaSO_4.2H_2O$). Sparingly soluble salts crystalize first in MD, thus acting as nuclei for crystallization of other minerals. Depending on the rate of crystal growth, PTFE-20 and M4 produced crystals of varying morphologies. Upon formation of gypsum, its periphery was decorated with growing crystals on its epitaxial. The crystal structures and crystallographic information of gypsum are presented in Figure 4 and Table 3, respectively. Interestingly, gypsum produced from each membrane was monoclinic with the C2/c space group. Similar findings were reported by Nazzareni *et al.* (2010). The resultant cubic crystal sizes were $2.5*10^{-3}$ mm^3 and $5.7*10^{-4}$ mm^3 for PTFE and M4 respectively. The crystal size was dependent on the growth rate. Based on process performance indicators, PTFE produced high water recovery rate with a 99.9% salt rejection compared to M4 (97.5%). Resultantly, the rate of solution supersaturation was higher in PTFE, ensuring high rate of crystal growth.

3.2.3 Powder x-ray diffraction (PXRD)

Powder x-ray diffraction (PXRD) was used to identify mineral products. This technique was used in conjunction to single crystal XRD because some of the solid product was present in a powder form. The experimental powder patterns for each membrane are presented in Figures 5A,B. Based on matched experimental pattern and databases (Figure 5), PTFE-20 produced gypsum ($CaSO_4.2H_2O$). These results agree with previously reported crystal XRD. In addition to gypsum, M4 produced an array of minerals identified as 29.66% arcanite (K_2SO_4), 21.77% cobalt sulfate VI), 1.55% halite (NaCl), 12.71% iron III) sulfate ($Fe_2(SO_4)_3$, monoclinic), 32.84% mikasite ($Fe_2(SO_4)_3$, rhombohedral), 0.79% nickel sulfate ($NiSO_4$), and 0.65% zinkosite ($ZnSO_4$). These mineral salts were grown on gypsum due to initiated nuclei formation on its surface. Gypsum is a sparingly soluble salt, forming first in MDC followed by an array of various salts. The differences calculated between the experimental pattern and the database patterns from M4 and PTFE-20 salts could be attributed to noise signals. Since M3 had little to no flux output, there was no crystalline solid for analysis.

3.3 Membrane deposition

Surface deposition in MDC application studies was inevitable. Therefore, establishing its impact on membrane performance is imperative (Chimanlal et al., 2022a). Scanning electron microscopy was used to evaluate salt deposition on the surface of the membranes (Figure 6). Furthermore, energy-dispersive x-ray spectrocopy (EDX) presented elemental composition of the deposition layer (Figure 7). M4 and PTFE-20 membranes were characterised by a cake layer. The cake layer was characterised by various mineral salts. Notably, potassium and iron were present in high concentrations. The EDS traces of gold were attributed to membrane coating during SEM preparation. These results provide further substantiation for the decline in membrane performance as a fuction of time. Furthermore, membrane fouling justified the decay in permeate flux and salt rejection. Notably, calcium was not detected, indicating little to no membrane scaling. Based on previously reported literature, a deposition layer on the membrane surface and its cause was ascribed to a decline in the feed velocity to the critical fouling velocity (Zhao et al., 2013). Moreover, a findings in literature reported considerable deposition layers caused flux decay due to 18% reduction in the mean pore size (Guillen-Burrieza et al., 2014).

4 Conclusion

The feasibility of synthesized PVDF-modified membranes was evaluated for the recovery of freshwater and minerals from AMD in MDC. The M4 membrane presented an average permeate flux of 1.459 kg m^{-2} hr^{-1} after 12.5 h. Comparatively, a commercial membrane (PTFE-20) achieved an average flux of 2.426 kg m^{-2}·h^{-1}. Additionally, M3 presented the poorest performance and did not attain supersaturation. The difference in the performance of M3 compared to M4 was largely attributed to the use of NPs in their respective matrices. The introduction of $fSiO_2$NPS improved membrane resistance to wetting. According to PXRD analysis, PTFE-20 produced gypsum, while M4 produced an array of mineral salts. These include cobalt sulphate, halite, and iron III) sulphate, among others. M3 was unable to recover mineral crystals due to poor recovery factors and a failure to reach supersaturation. Its poor performance was a consequence of membrane structural damage and foulant deposition. Nonetheless, SEM micrographs revealed some deposition on the membrane surface confirming the susceptibility of all membranes to fouling during MDC application. The incorporation of NPs into the membrane matrix afforded a satisfactory performance of M4 in MDC. However, further investigation into the longevity of the membrane's performance is required, as slight membrane wetting was responsible for an increased distillate conductivity. The evidence presented herein endorses the incorporation of $fSiO_2$NPS towards improved rate of water recovery with high salt rejection, thus ensuring crystal nuclei formation and growth. This study thus provided further motivation to enhance membrane performance through incorporation of NPs. Additionally, evidence for the use of MDC toward the treatment of harsh AMD has been unlocked.

Data availability statement

The original contributions presented in the study are included in the article/supplementary material, further inquiries can be directed to the corresponding authors.

Author contributions

HR and CQ-J conceptualized and supervised the study, LN supervised the study and curated date and corrected manuscript, IC conducted the study and wrote the draft. All authors contributed to the article and approved the submitted version.

Funding

This research was funded by the Ministry of Foreign Affairs of Denmark (MFA) through Danida Fellowship Centre (DFC) project no. 20-M01AAU and DANIDA1 "Membrane crystallization for water and mineral recovery". The APC was funded by the University of the Witwatersrand.

Conflict of interest

The author(s) LN declared that they were an editorial board member of Frontiers, at the time of submission. This had no impact on the peer review process and the final decision.

The remaining authors declare that the research was conducted in the absence of any commercial or financial relationships that could be construed as a potential conflict of interest.

Publisher's note

All claims expressed in this article are solely those of the authors and do not necessarily represent those of their affiliated organizations, or those of the publisher, the editors and the reviewers. Any product that may be evaluated in this article, or claim that may be made by its manufacturer, is not guaranteed or endorsed by the publisher.

References

Akcil, A., and Koldas, S. (2006). Acid Mine Drainage (AMD): causes, treatment and case studies. *J. Clean. Prod.* 14 (12), 1139–1145. doi:10.1016/j.jclepro.2004.09.006

Alegbe, M. J., Ayanda, O., Ndungu, P., Nechaev, A., Fatoba, O., and Petrik, L. (2019). Physicochemical characteristics of acid mine drainage, simultaneous remediation and use as feedstock for value added products. *J. Environ. Chem. Eng.* 7 (3), 103097. doi:10.1016/j.jece.2019.103097

Ali, A., Quist-Jensen, C. A., Macedonio, F., and Drioli, E. (2015). Application of membrane crystallization for minerals' recovery from produced water. *Membranes* 5, 772–792. doi:10.3390/membranes5040772

Alvarez, R., Nievergelt, P. P., Slyshkina, E., Müller, P., Alberto, R., and Spingler, B. (2020). Single crystal growth of water-soluble metal complexes with the help of the nano-crystallization method. *Dalton Trans.* 49 (28), 9632–9640. doi:10.1039/d0dt01236j

Anekwe, S., and Isa, Y. M. (2023). Bioremediation of acid mine drainage – Review. *Alexandria Eng. J.* 65, 1047–1075. doi:10.1016/j.aej.2022.09.053

Bruker (2021). *APEX4version 2021.4-1 data collection software which includes SAINT version 8.40B, SADABS-2016/2 and XPREP version 2014/2.* ' Madison, Wisconsin, USA: Bruker AXS Inc.)

Chimanlal, I., Lesaoana, M., and Richards, H. (2022b). Chemical modification of Macadamia -derived activated carbon for remediation of selected heavy metals from wastewater. *Miner. Eng.* 184, 107663. doi:10.1016/j.mineng.2022.107663

Chimanlal, I., Nthunya, L. N., Mahlangu, O. T., Kirkebæk, B., Quist-Jensen, C. A., Ricahrds, H., et al. (2023). Nanoparticle-Enhanced PVDF Flat-Sheet Membranes for Seawater Desalination in Direct Contact Membrane Distillation. *Membranes* 13 (317), 317–17. doi:10.3390/membranes13030317

Chimanlal, I., Nthunya, L. N., Quist-Jensen, C., and Richards, H. (2022a). Membrane distillation crystallization for water and mineral recovery: the occurrence of fouling and its control during wastewater treatment. *Front. Chem. Eng.* 4, 1–14. doi:10.3389/fceng.2022.1066027

Choi, Y., Naidu, G., Jeong, S., Lee, S., and Vigneswaran, S. (2018) 'Effect of chemical and physical factors on the crystallization of calcium sulfate in seawater reverse osmosis brine', *Desalination*, 426(2017), pp. 78–87. doi:10.1016/j.desal.2017.10.037

Choi, Y., Naidu, G., Lee, S., and Vigneswaran, S. (2020). Recovery of sodium sulfate from seawater brine using fractional submerged membrane distillation crystallizer. *Chemosphere* 238, 124641. doi:10.1016/j.chemosphere.2019.124641

Dhamsaniya, M., Sojitra, D., Modi, H., Shabiimam, M., and Kandya, A. (2022). A review of the techniques for treating the landfill leachate. *Mater. Today Proc.* 77, 358–364. doi:10.1016/j.matpr.2022.11.496

Dolomanov, O. V., Bourhis, L. J., Gildea, R. J., Howard, J. A. K., and Puschmann, H. (2009). OLEX2: a complete structure solution, refinement and analysis program. *J. Appl. Crystallogr.* 42 (2), 339–341. doi:10.1107/s0021889808042726

Edwie, F., and Chung, T.-S. (2013). Development of simultaneous membrane distillation–crystallization (SMDC) technology for treatment of saturated brine. *Chem. Eng. Sci.* 98, 160–172. doi:10.1016/j.ces.2013.05.008

Egashira, R., Tanabe, S., and Habaki, H. (2012). Adsorption of heavy metals in mine wastewater by Mongolian natural zeolite. *Procedia Eng.* 42, 49–57. doi:10.1016/j.proeng.2012.07.394

García-Lorenzo, M. L., Marimón, J., Navarro-Hervás, M. C., Pérez-Sirvent, C., Martínez-Sánchez, M. J., and Molina-Ruiz, J. (2016). Impact of acid mine drainages on surficial waters of an abandoned mining site. *Environ. Sci. Pollut. Res.* 23 (7), 6014–6023. doi:10.1007/s11356-015-5337-2

Gontarek-Castro, E., Castro-Muñoz, R., and Lieder, M. (2022). New insights of nanomaterials usage toward superhydrophobic membranes for water desalination via membrane distillation: A review. *Crit. Rev. Environ. Sci. Technol.* 52 (12), 2104–2149. doi:10.1080/10643389.2021.1877032

Greve, P., Kahil, T., Mochizuki, J., Schinko, T., Satoh, Y., Burek, P., et al. (2018). Global assessment of water challenges under uncertainty in water scarcity projections. *Nat. Sustain.* 1 (9), 486–494. doi:10.1038/s41893-018-0134-9

Gryta, M. (2008). Fouling in direct contact membrane distillation process. *J. Membr. Sci.* 325 (1), 383–394. doi:10.1016/j.memsci.2008.08.001

Guillen-Burrieza, E., Ruiz-Aguirre, A., Zaragoza, G., and Arafat, H. A. (2014). Membrane fouling and cleaning in long term plant-scale membrane distillation operations. *J. Membr. Sci.* 468, 360–372. doi:10.1016/j.memsci.2014.05.064

Jiang, X., Lu, D., Xiao, W., Ruan, X., Fang, J., and He, G. (2016). Membrane assisted cooling crystallization: process model, nucleation, metastable zone, and crystal size distribution. *AIChE J.* 62 (3), 829–841. doi:10.1002/aic.15069

Lu, D., Li, P., Xiao, W., He, G., and Jiang, X. (2017). Simultaneous recovery and crystallization control of saline organic wastewater by membrane distillation crystallization. *AIChE J.* 63, 2187–2197. doi:10.1002/aic.15581

Nazzareni, S., Comodi, P., Bindi, L., and Dubrovinsky, L. (2010). The crystal structure of gypsum-II determined by single-crystal synchrotron X-ray diffraction data. *Am. Mineralogist* 95 (4), 655–658. doi:10.2138/am.2010.3452

Nthunya, L. N., Gutierrez, L., Derese, S., Nxumalo, E. N., Verliefde, A. R., Mamba, B. B., et al. (2019). A review of nanoparticle-enhanced membrane distillation membranes: membrane synthesis and applications in water treatment. *Chem. Technol. Biotechnol.* 94 (9), 2757–2771. doi:10.1002/jctb.5977

Olatunji, S. O., and Camacho, L. M. (2018). Heat and mass transport in modeling membrane distillation configurations: A review. *Front. Energy Res.* 6, 1–18. doi:10.3389/fenrg.2018.00130

Ondrasek, G., and Rengel, Z. (2021). Environmental salinization processes: detection, implications and solutions. *Sci. Total Environ.* 754, 142432. doi:10.1016/j.scitotenv.2020.142432

Sheldrick, G. (2015a). Crystal structure refinement with SHELXL. *Acta Crystallogr. Sect. C* 71 (1), 3–8. doi:10.1107/S2053229614024218

Sheldrick, G. (2015b). SHELXT - Integrated space-group and crystal-structure determination. *Acta Crystallogr. Sect. A* 71 (1), 3–8. doi:10.1107/S2053273314026370

Sparenberg, M. C., Ruiz Salmón, I., and Luis, P. (2020). Economic evaluation of salt recovery from wastewater via membrane distillation-crystallization. *Sep. Purif. Technol.* 235, 116075. doi:10.1016/j.seppur.2019.116075

Stein, S., Michael, H. A., and Dugan, B. (2021). Injection of desalination brine into the saline part of the coastal aquifer; environmental and hydrological implications. *Water Res.* 207, 117820. doi:10.1016/j.watres.2021.117820

Yadav, A., Labhasetwar, P. K., and Shahi, V. K. (2022). Membrane distillation crystallization technology for zero liquid discharge and resource recovery: opportunities, challenges and futuristic perspectives. *Sci. Total Environ.* 806, 150692. doi:10.1016/j.scitotenv.2021.150692

Zhao, Z.-P., Zhu, C. Y., Liu, D. Z., and Liu, W. F. (2011). Concentration of ginseng extracts aqueous solution by vacuum membrane distillation 2. Theory analysis of critical operating conditions and experimental confirmation. *Theory analysis Crit. operating Cond. Exp. confirmation' Desalination* 267 (2), 147–153. doi:10.1016/j.desal.2010.09.017

Zhao, Z. P., Xu, L., Shang, X., and Chen, K. (2013). Water regeneration from human urine by vacuum membrane distillation and analysis of membrane fouling characteristics. *Sep. Purif. Technol.* 118, 369–376. doi:10.1016/j.seppur.2013.07.021